Original Paper

phys. stat. sol. (b) **243**, No. 9, 2111–2116 (2006) / **DOI** 10.1002/pssb.200666814

Pressure induced high spin to low spin transition in magnesiowüstite

Taku Tsuchiya[1], **Renata M. Wentzcovitch**[*, 2], **Cesar R. S. da Silva**[3], **Stefano de Gironcoli**[4, 5] and **Jun Tsuchiya**[1]

[1] Geodynamics Research Center, Ehime University, 2-5 Bunkyo-cho, Matsuyama 790-8577, Japan
[2] Department of Chemical Engineering and Materials Science, University of Minnesota, MN 55455, USA
[3] Minnesota Supercomputing Institute for Digital Technology and Advanced Computations, University of Minnesota, MN 55455, USA
[4] Scuola Internazionale Superiore di Studi Avanzati, Trieste, Italy
[5] DEMOCRITOS National Simulation Center, Trieste, Italy

Received 28 April 2006, accepted 16 May 2006
Published online 10 July 2006

PACS 71.15.Mb, 71.27.+a, 75.20.Ck

Using a rotationally invariant formulation of LDA + U, we report a successful study of the high spin (HS)/low spin (LS) transition in low solute concentration magnesiowüstite (Mw), $(Mg_{1-x}Fe_x)O$, ($x < 20\%$), the second most abundant phase in Earth's lower mantle. The HS state crosses over smoothly to the LS state passing through an insulating mixed spins state where properties change continuously, as seen experimentally. These encouraging results indicate this method should enable first principles studies of strongly correlated iron-bearing minerals, a major class of mineral physics problems.

Magnesiowüstite (Mw), $(Mg_{1-x}Fe_x)O$, is believed to be the major mineral phase in Earth's lower mantle (LM) after ferrosilicate perovskite, $(Mg_{1-x}Fe_x)SiO_3$ (hereafter Pv) [1]. The effect of iron incorporation on the thermodynamic and elastic properties of these minerals is a crucial issue in mineral physics. High spin to low spin (HS/LS) transitions in iron have been observed by in situ X-ray emission spectroscopy (XES) and Mössbauer spectroscopy from 40 to 70 GPa in Mw [2, 3] and from 70 and 120 GPa in Pv [4–6] at room temperature. This transition is accompanied by volume reduction [3] and changes in these minerals' optical absorption spectrum. These can produce seismic velocity anomalies, variations in Mg-Fe^{2+} partitioning between Mw and Pv, changes in radiative heat conductivity, and compositional layering [2, 4, 7, 8]. The elastic signature of this transition has now been partially explored [3], but there is still much to be quantified to pin down the effects of this spin transition on these properties. At the same time, the strongly correlated behavior of iron oxide has deterred the quantification of these changes by density functional calculations based on the local spin density (LSDA) and spin-polarized generalized gradient approximations (σ-GGA). These approaches and phenomenological models [9] produce incorrectly a metallic HS ground state and then successive spin collapses across the transition [10, 11].

Here we use a rotationally invariant version of the LDA + U approach implemented in the planewave pseudopotential method, where U is calculated in an internally consistent way [12]. This approach has been very successful in describing the electronic and structural properties of FeO, wüstite, under pressure [12], an antiferromagnetic insulator with a Néel temperature of 198 K. Computations were performed using the local density approximation (LDA) [13, 14]. The oxygen pseudopotential was generated by the

* Corresponding author: e-mail: wentzcov@cems.umn.edu, Phone: (612) 625-6345, Fax: (612) 626-7246

method of Troullier–Martins [15] with core radii $r(2s) = r(2p) = 1.45$ a.u. in the configuration $2s^2\,2p^4$ with p locality. The magnesium pseudopotential was generated by the method of von Barth-Car [16]. Five configurations, $3s^2\,3p^0$, $3s^1\,3p^1$, $3s^1\,3p^{0.5}\,3d^{0.5}$, $3s^1\,3p^{0.5}$, $3s^1\,3d^1$ with decreasing weights 1.5, 0.6, 0.3, 0.3, and 0.2 respectively were used. Core radii were $r(3s) = r(3p) = r(3d) = 2.5$ a.u. with d locality. These pseudopotentials have been successfully used for MgO, silicate perovskite, and post-perovskite [17–19]. The ultrasoft pseudopotential for iron was generated using the modified Rappe–Rabe–Kaxieas-Joannopoulos scheme [20]. Core radii were $r(4s) = (2.0, 2.2)$, $r(4p) = (2.2, 2.3)$, and $r(3d) = (1.6, 2.2)$ a.u. in the configuration $3d^7\,4s^1$, where the first is the norm-conserving core radius and the second is the ultrasoft one in unit a.u. All-electron potential pseudized at $r_c < 1.7$ was taken as a local potential. The plane wave energy cutoff was chosen as 70 Ry. Brillouin zone sampling for electronic states was carried out on 8 k-points for the cubic supercell containing 64 atoms ($2 \times 2 \times 2$ of the conventional unit cell). Equivalent k-points were used in the 128 and 216 atom calculations for Mw with $X_{Fe} = 3.125\%$. We used the rotationally invariant LDA + U method [12, 21, 22] to describe the electronic structure of iron oxide correctly. Values of the effective Hubbard U parameter have been determined at each volume for each of the three concentration, $X_{Fe} = 3.125$, 12.5, 18.75%, using a linear response approach to the variations of Fe-3d occupancies subjected to localized perturbations [12]. This approach refines the perturbative formulation proposed by Pickett et al [23]. Most of our calculations were performed in 64-atoms supercells, but two calculations were also carried out in 128 and 216 atom supercells for convergence tests. We investigated Mw with $X_{Fe} = 3.125\%$, 12.5% and 18.75%, the latter being similar to the experimentally investigated concentration, 17% [2, 3]. The atomic configurations were ordered and homogeneous with Fe^{2+}s positioned as far from each other as possible. All atomic positions were completely relaxed in these LDA + U calculations. The Hubbard U was computed from the inverse density response matrices (interacting and non-interacting) obtained by applying localized potential shifts on single Hubbard sites [12]. Supercell size effects on U were estimated by using elements of the small density response matrices (from 64 atom supercells in all cases but also from 128 and 216 for) to construct response matrices corresponding to 512 atom supercells. This procedure [12] nicely captures size effects on U.

Us computed as functions of pressure for these three concentrations are shown in Fig. 1. They are approximately concentration independent for X_{Fe} up to 18.75%. The increase of Us with pressure does not reflect an increase in correlation strength. First, Us and their pressure derivatives depend on the definition of the strongly correlated orbitals. We have used atomic like d-(pseduo)orbitals but other definitions are also possible [24]. Despite this non-uniqueness, total energies are always computed consistently using the same orbitals employed in the derivation of U, and their changes are physically meaningful. Second, in the Hubbard model it is the ratio U/Δ, where Δ is the d bandwidth, that characterizes the correlation strength, $U/\Delta \gg 1$ ($U/\Delta \ll 1$) corresponding to the strong (weak) correlated limit. For $X_{Fe} = 12.5\%$, $\Delta^{-1} \cdot \mathrm{d}\Delta/\mathrm{d}P$ is ~ 0.01, which is approximately one order of magnitude larger than $U^{-1} \cdot \mathrm{d}U/\mathrm{d}P$, indicating, as expected, a decrease of correlation with pressure. Finally, the intermediate

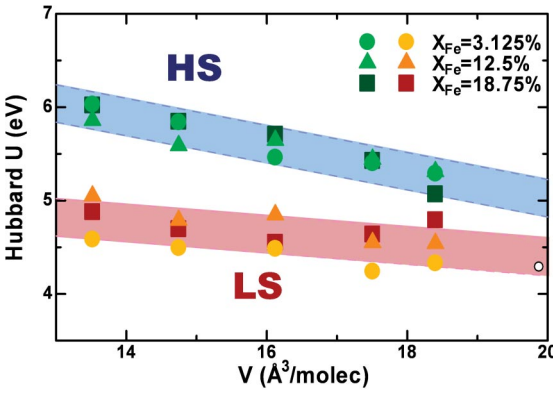

Fig. 1 (online colour at: www.pss-b.com) Computed Hubbard U as function of pressure for ferromagnetic HS and LS states. Us for antiferromagnetically ordered spins fall within these same ranges. $U_{HS} = -[0.15\,V - 7.92] \pm 0.2$ eV and $U_{LS} = -[0.06\,V - 5.61] \pm 0.2$ eV, where V is the volume per formula unit in Å^3. Variations of U within these ranges have minor influence on the structural properties. Open circle is U for HS iron in FeO [12].

$S = 1$ spin state was never stabilized in a self-consistent cycle, regardless of the initial occupation of iron d-orbitals. The final stable state was always found to have $S = 0$ or 2, depending on pressure.

The electronic structure of Mw within the LDA + U approach is drastically different from that obtained using conventional LSDA. Figures 2A,B show the projected density of states from standard LSDA and LDA + U calculations, respectively, for Mw in the HS state with iron concentration 12.5%. Gray lines represent O 2p states. In the LSDA calculation, blue are majority, green and orange are minority t_{2g} and e_g 3d states of iron, respectively. In conventional LSDA calculations, the Fermi level (dashed red line) falls in the middle of the minority t_{2g} state, that is, the system is metallic. In LDA + U calculations the octahedral symmetry breaks and a gap of 3 eV opens within the minority t_{2g} states. One t_{2g} state (dark green) remains below the Fermi level and two others (light green) become empty. A splitting also occurs within the e_g state. The orange states split into dark and light orange. LDA + U also increases hybridization between majority 3d states and O 2p states. 3d states participate in the entire 2p valence bands. These details in the electronic structure of HS Mw are consistent with those observed in the electronic structure of FeO [25]. A strong absorption corresponding to this 3d(Fe)–2p(O) → 3d(Fe) transition is expected. Considering shorter Fe–O bond length in Mw compared to that in pure FeO, the calculated gap of 3 eV is in reasonable agreement with an experimental absorption with stronger line around 2.4 eV in FeO [26]. The large mixing between majority Fe d states and O p states over a wide range of energies and the small contribution of O at the top of the valence band are also similar to these features observed in the density of states of FeO [12]. They point to a moderate charge transfer character in the insulating state. However, in FeO iron–iron interaction is essential and causes other several effects not seen here [12]. Figures 2C, D are density of states for LS Mw. Conventional LSDA calculations (Fig. 2C) produce an unrealistic narrow gap between occupied t_{2g} and empty e_g states. LDA + U opens a gap approximately 2.6 eV wide between them. No Jahn–Teller distortion or symmetry breaking appears within the t_{2g} or e_g states (Fig. 2D). Hybridization between d and O p states is not enhanced as much in this case [27]. Although more information regarding the oscillation strength for electronic excitations is necessary, the moderate charge transfer gaps for both, HS and LS Mw, suggest that the optical absorption spectrum of Mw should display a *red shift* across the spin transition, not a *blue shift* as estimated by simple crystal field arguments [2, 28].

The dependence of the transition pressure, P_t, on X_{Fe} has already been investigated experimentally across the entire range of compositions in this isomorphous alloy [3, 29]. It has been shown consistently that P_t increases with X_{Fe} in high-concentration Mw ($X_{Fe} > 25\%$). Figure 3A shows our calculated enthalpy differences between the LS and HS states ($\Delta H_{LS\text{-}HS}$) obtained in static calculations for three different concentrations. Within our accuracy and for these small values of X_{Fe}, the transition pressure (P_t) is 32 ± 2 GPa and does not depend on X_{Fe}. This result implies that chemical, exchange, and elastic interactions between neighboring irons are negligible in low concentration Mw. Therefore, up to $X_{Fe} = 18.75\%$, a particular HS iron should always undergo the spin transition at the same P_t, irrespective of the state of neighboring irons, be they LS or HS, parallel or anti-parallel. This implication is verified in Fig. 3B, which shows the difference in enthalpy, ΔH, in $X_{Fe} = 18.75\%$ Mw between states with various fractions of coexisting LS and HS irons, represented by $n = n_{LS}/(n_{HS}+n_{LS})$. This implies that at 0 K and up to $X_{Fe} = 18.75\%$, the spin transition is sharp and should be approximately concentration independent, as shown in Fig. 3A. In addition, it points to the possibility of the high temperature stabilization of a mixed spin (MS) state by an increase in HS/LS configuration entropy, $S_{LS–HS}$.

Static compression curves for $X_{Fe} = 18.75\%$ in various MS states are shown in Fig. 3C along with measurements at room temperature in 17% iron Mw [3]. The latter changes smoothly ($54 < P_t < 67$ GPa) and spans the predicted compression curves of $0 < n < 1$. This appears to be evidence of a continuous increase in LS fraction, n, that could originate in pure thermodynamic equilibrium, as indicated by our calculations. The wide transition pressure range could also have a contribution from hysteresis, since there are large octahedral volume changes associated with the transition. Experiments at higher temperatures should distinguish these effects: hysteresis should decrease the transition pressure range with temperature, thermodynamic equilibrium should increase the same. Experimental and theoretical compression curves of the initial HS and final LS states also agree quite well below ~40 GPa (HS state) and

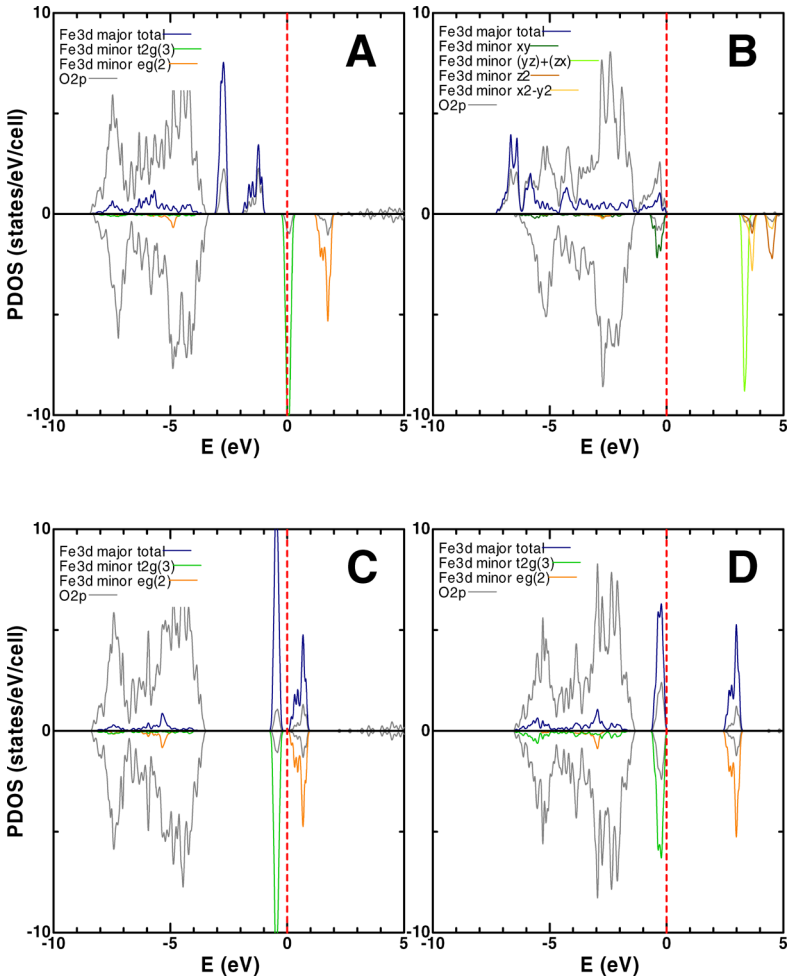

Fig. 2 (online colour at: www.pss-b.com) Projected density of states of Mw in the HS state from standard A) LSDA and B) LDA + U calculations for iron concentration 12.5%, respectively. The same for the LS state for C) LSDA and D) LDA + U. See text for detailed description.

above ~60 GPa (LS state). The slight underestimation of calculated volumes at low pressures is typical of static calculations lacking zero point motion and thermal effects at 300 K. Up to $X_{Fe} = 18.75\%$; we find the zero pressure equilibrium volume, V_0, in the HS state increases linearly with $dV_0/dX_{Fe} = 10.5 \times 10^{-3}$ cm^3/mol, consistent with experimental observations, $dV_0/dX_{Fe} = 8.9\times10^{-3}$ cm^3/mol [30]. The zero pressure bulk modulus, $dB_0/dX_{Fe} = 0.28$ GPa for HS Mw and 1.06 GPa for LS Mw, also increases and is in good agreement with the quite X_{Fe}-insensitive B_0 measured for HS Mw [30]. A considerable volume reduction of 4.2% can be seen across the spin transition at $X_{Fe} = 18.75\%$ in Fig. 3C. For $X_{Fe} \leq 18.75\%$, this volume reduction is linear in X_{Fe} and in n, and can be represented by $d\Delta V/dX_{Fe} = -2.22 \times 10^{-2}\ nX_{Fe}$ cm^3/mol. An increase in bulk modulus from 297 to 313 GPa is seen at $X_{Fe} = 18.75$ % and at the static transition pressure. Similar to the volume change, the change in B_0 can be expressed as $d\Delta B/dX_{Fe} = 0.84\ nX_{Fe}$ GPa.

The behavior of Mw for $X_{Fe} > 18.75\%$ could not be easily addressed. Iron–iron interactions are no longer negligible and P_t becomes strongly dependent of concentration and on magnetic state. For instance, in Mw with $X_{Fe} = 25\%$ we identified a tendency for structural ordering, anti-ferromagnetic alignment, and we found $P_t > 125$ GPa. This tendency parallels experimental observations in Mw with

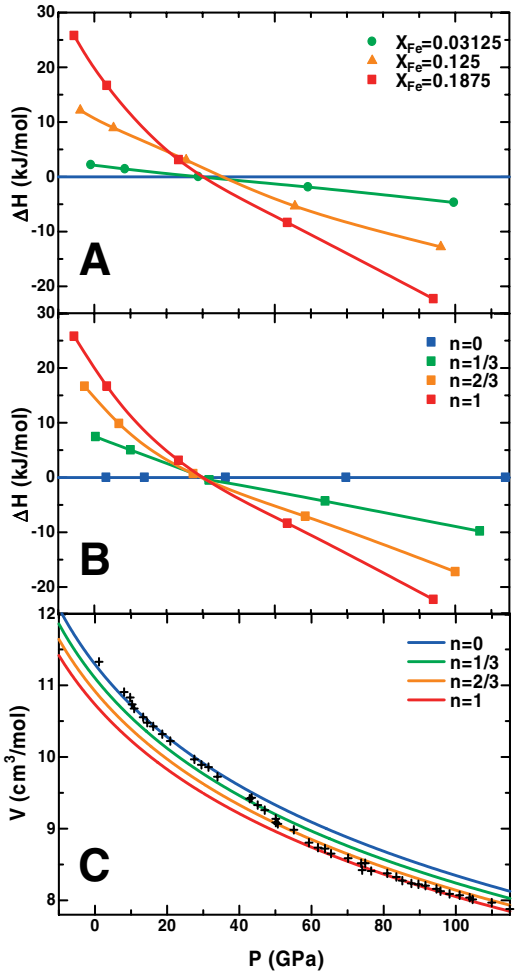

Fig. 3 (online colour at: www.pss-b.com) Static enthalpy differences between LS and HS phases at three different iron concentrations (A). Enthalpy differences in Mw with $X_{Fe} = 18.75\%$, between states with various fractions of coexisting HS and LS irons, $n = n_{LS}/(n_{HS} + n_{LS})$, and the HS state (B). The reference green line corresponds to the enthalpy of all irons in the HS state ($n = 0$). Pressure–volume curves (C) for the same n's as shown in (B). Experimental results [3] at 300 K for Mw with $X_{Fe} = 17\%$ are represented by +. The central thin black curve corresponds to MgO.

$X_{Fe} = 60\%$, where $84 < P_t < 102$ GPa [3] and with $X_{Fe} = 100\%$, where no spin transition up to 143 GPa [29] has been reported. A similar calculation in FeO has not found any spin transition up to 300 GPa either [31]. Mw with $X_{Fe} = 50\%$ and 60% were also reported to dissociate into iron reach and iron poor phases [32], a clear consequence of iron–iron interactions. These interactions, that involve cooperative Jahn–Teller distortions, i.e., orbital ordering [12], prevented us from extending our low-solute concentration treatment to higher concentrations. Although X_{Fe} in Mw in the LM is expected to be ~20%, iron partitioning between Mw and Pv could be affected by the spin transition [2, 4].

In summary, the pressure induced spin transition in a strongly correlated iron-bearing mineral is successfully described by a first principles approach. In Mw, the pressure induced HS/LS transition is direct from insulating $S = 2$ to $S = 0$, is expected to display a red shift in the optical gap. For higher solute concentrations, interactions between irons that could lead to complex ordering phenomena, or even phase separation [33], may occur. Our encouraging results indicate that it is possible now to explore by first principles iron bearing minerals, a major class of mineral physics problems.

Acknowledgements We acknowledge P. B. Allen for stimulating discussions. RMW is grateful to the Department of Geosciences at Stony Brook University for hospitality during the final stages of this research. Research was supported by NSF grants EAR-0135533, EAR-0230319, ITR-0325218 (ITAMIT), ITR-0428774 (*VLab*), and the U. of Minnesota MRSEC. TT was also partly supported by the Japan Society for the Promotion of Science (JSPS).

References

[1] G. R. Helffrich and B. J. Wood, Nature **412**, 501 (2001).
[2] J. Badro, Science **300**, 789 (2003).
[3] J.-F. Lin et al., Nature **436**, 377 (2005).
[4] J. Badro et al., Science **305**, 383 (2004).
[5] J. Li et al., PNAS **101**, 14027 (2004).
[6] J. M. Jackson et al., Am. Mineral. **90**, 199 (2005).
[7] E. S. Gaffney and D. L. Anderson, J. Geophys. Res. **78**, 7005 (1973).
[8] D. M. Sherman, J. Geophys. Res. **96**, 14299 (1991).
[9] W. Sturhahn, J. M. Jackson, and J.-F. Lin, Geophys. Res. Lett. **32**, L12307 (2005).
[10] D. M. Sherman and H. J. F. Jansen, Geophys. Res. Lett. **22**, 1001 (1995).
[11] R. Cohen, I. I. Mazin, and D. G. Isaak, Science **275**, 654 (1997).
[12] M. Cococcioni and S. de Gironcoli, Phys. Rev. B **71**, 035105 (2005).
[13] D. Ceperley and B. Alder, Phys. Rev. Lett. **45**, 566 (1980).
[14] J. P. Perdew and A. Zunger, Phys. Rev. B **23**, 5048 (1981).
[15] N. Troullier and J. L. Martins, Phys. Rev. B **43**, 1993 (1991).
[16] U. von Barth and R. Car, unpublished.
[17] B. B. Karki, R. M. Wentzcovitch, S. de Gironcoli, and S. Baroni, Science **286**, 1705 (1999).
[18] R. M. Wentzcovitch, B. B. Karki, and M. Cococcioni S. de Gironcoli, Phys. Rev. Lett. **92**, 018501 (2004).
[19] T. Tsuchiya, J. Tsuchiya, K. Umemoto, and R. M. Wentzcovitch, Earth Planet. Sci. Lett. **224**, 241 (2004).
[20] A. M. Rappe, K. M. Rabe, E. Kaxiras, and J. D. Joannopoulos, Phys. Rev. B **41**, 1227 (1990).
[21] V. I. Anisimov, J. Zaanen, and O. K. Andersen, Phys. Rev. B **44**, 943 (1991).
[22] A. I. Liechtenstein, V. I. Anisimov, and J. Zaanen, Phys. Rev. B **52**, R5467 (1995).
[23] W. E. Pickett, S. C. Erwin, and E. C. Ethridge, Phys. Rev. B **58**, 1201 (1998).
[24] S. Fabris et al., Phys. Rev. B **71**, 041102 (2005).
[25] Korotin et al., Phys. Rev. B **49**, 6548 (1994). They investigated electronic structure of HS Mw having $X_{Fe} = 0.125$ with empirical U parameter at cell constant of 4.21 Å. They also found tetragonal distortion after applying LDA + U.
[26] I. Balberg and H. L. Pinch, J. Magn. Magn. Mater. **7**, 12 (1978).
[27] Computations were performed using the Quantum-ESPRESSO package (opEn-Source Package for Research in Electronic Structure, Simulation, and Optimization http://www.quantum-espresso.org). This is an initiative of the DEMOCRITOS National Simulation centre (http://www.democritos.it) for the development of open-source scientific software.
[28] R. G. Burns, Mineralogical Application of Crystal Field Theory (Cambridge University Press, Cambridge, 1993).
[29] J. Badro et al., Phys. Rev. Lett. **83**, 4101 (1999).
[30] S. D. Jacobsen et al., J. Geophys. Res. **107**, 2037 (2002).
[31] S. Gramsch, R. Cohen, and S. Savrasov, Am. Mineral. **88**, 257 (2003).
[32] L. S. Dubrovinski et al., Science **289**, 430 (2000).
[33] R. Boehler, Rev. Geophys. **38**, 221 (2000).

